Indonesian Physical Review
Volume 09 Issue 02, May 2026
P-ISSN: 2615-1278, E-ISSN: 2614-7904

Synthesis of Magnetite/Activated Carbon Nanocomposites for the Removal of Lead and Methylene Blue

Mina Devika Setiana[1], Yap Wing Fen[2], Arif Hidayat[1], ST. Ulfawanti Intan Subadra[1], Ahmad Taufiq[1]*
[1]*Department of Physics, Faculty of Mathematics and Natural Sciences, Universitas Negeri Malang, Jl. Semarang 5 Malang 65145, Indonesia*
[2]*Department of Physics, Faculty of Science, Universiti Putra Malaysia, 43400 UPM, Serdang, Selangor, Malaysia*

Corresponding Author's E-mail: ahmad.taufiq.fmipa@um.ac.id

Article Info

Article info:
Received: 21-01-2026
Revised: 03-04-2026
Accepted: 20-04-2026

Keywords:
Magnetite/activated carbon; Nanocomposites; Adsorption; Lead; Methylene blue

How To Cite:
M. D. Setiana, Y. W. Fen, A. Hidayat, S. U. I. Subadra, and A. Taufiq, "Synthesis of Magnetite/Activated Carbon Nanocomposites for the Removal of Lead and Methylene Blue", Indonesian Physical Review, vol. 9, no. 2, p 286-301, 2026.

DOI:
https://doi.org/10.29303/ipr.v9i2.651.

Abstract

Water pollution from industrial waste, such as lead and methylene blue (MB), has serious impacts on aquatic life and human health. In addition, existing methods are less effective for waste treatment and are costly to operate. Therefore, this study aims to develop magnetite/activated carbon nanocomposites based on natural materials as adsorbents. The XRD diffraction pattern showed broadened peaks and the highest crystalline peaks at 2θ = 20°–26° and 35.5° for activated carbon and magnetite, respectively. The nanocomposite formation was confirmed from the EDX spectrum, which showed the presence of Fe, O, and C elements, as well as from the FTIR spectrum, which detected the presence of Fe–O, C–H, C=C, C=O, and O–H functional groups. Furthermore, based on the SEM results, the nanocomposites were found to be spherical and porous, with an average particle size of 35.53 ± 0.83 nm. Meanwhile, the BET results showed that the nanocomposites had a total pore volume of 0.333 cm^3/g. The kinetics of lead adsorption reached equilibrium in 25 minutes with an efficiency of 99.51%. The adsorption of MB reached equilibrium in 20 minutes, with an efficiency of 97.02%. The results of the kinetic analysis showed that the adsorption of lead and MB both fit the pseudo-second order (PSO) modeling with adsorption capacities (q_e) of 11.6550 mg/g and 7.3421 mg/g, respectively. Based on these results, the magnetite/activated carbon nanocomposites are promising as an alternative adsorbent due to their high efficiency, practicality, and magnetic separation capabilities.

Introduction

Rapid industrial development poses a serious threat to the environment, especially to aquatic environments [1]. Currently, many irresponsible industries discharge untreated industrial waste directly into water. The Indonesian Central Bureau of Statistics reports that 38 rivers in Indonesia are severely polluted by waste from large industrial and household activities [2]. Industrial waste is known to contain hazardous contaminants, including lead (Pb) and methylene blue (MB). This is supported by reports stating that 10%–15% of MB found in waters is generated from 8,000 kg/day of textile production [3]. Meanwhile, lead pollution is reported to originate from the battery, mining, and manufacturing industries [4,5]. Under these conditions, living things may be exposed to dangerous contaminants. Previous research reported that one in four children in Indonesia has been exposed to lead, with accumulated blood lead levels exceeding 10 µg/dL [6]. Pb and MB themselves are known to have toxic characteristics, are non-biodegradable, and cause health problems [7–9]. Therefore, exposure to lead and MB can cause disruption of vital organ function, poisoning, cardiovascular disease, cancer, jaundice, and red blood cell abnormalities [10–12].

Several methods have been developed to address lead and MB contamination, such as ion exchange, chemical precipitation, coagulation, membrane filtration, and solvent extraction [13]. However, these methods still have limitations, including complicated mechanisms, high costs, high energy requirements, and longer processes, so alternative solutions are needed to overcome water pollution [14]. Therefore, this study uses the adsorption method because it has the advantages of being simpler, having high efficiency, and not requiring large amounts of energy compared to other methods [15,16]. The adsorption method is reported to have high performance by utilizing adsorbent materials, such as activated carbon.

Activated carbon is widely used as an adsorbent because it has a high surface area and porosity, and contains numerous oxygen and hydroxyl groups that enhance its hydrophilic properties, thereby increasing adsorption capacity [14,17,18]. The report showed that activated carbon successfully adsorbed iron and lead with adsorption capacities of 9.67 mg/g and 10.04 mg/g [19]. However, in its application, activated carbon is difficult to separate from pollutants, which can lead to new environmental problems. Therefore, this study modified activated carbon by adding another functional material, magnetite. Magnetite nanoparticles possess superior magnetic properties, making them useful in separating adsorbent materials. In addition, magnetite has high biocompatibility and low toxicity, making it safer for the environment [20,21]. Previous studies reported that magnetite/activated carbon as lead and MB adsorption had efficiencies of 86.87% and 95.2%, respectively [22,23]. Other research also succeeded in synthesizing magnetite combined with granular activated carbon, showing an adsorption efficiency of perfluorooctanoic acid of 79.1% [24]. This value is higher than the efficiency of pure magnetite and granular activated carbon at 10.1% and 58.9%, respectively. Although research on magnetite and activated carbon has been widely conducted, discussion of their adsorption by both materials remains limited to certain pollutants, emphasizes removal efficiency, and does not conduct in-depth kinetic analysis. Therefore, unfortunately, these adsorbent materials are synthesized using chemicals such as $C_7F_{15}COOH$, $FeCl_2.4H_2O$, $FeCl_3.7H_2O$, and NH3.H2O, and excessive use of these chemicals can lead to secondary pollutants in water and increase manufacturing costs. Based on the above, this research aims to synthesize magnetite/activated carbon nanocomposites using natural iron sand and coconut shells for adsorbing lead and methylene blue.

The use of these two natural materials is a novelty offered in this research. Iron sand is known to have a high magnetite content in bulk form [25]. Meanwhile, coconut shells were chosen because they contain 35-45% lignin and 23-43% cellulose, both of which have high carbon content [26]. By utilizing natural materials and biomass waste as precursors, it has the potential to lower production costs, reduce biomass waste, and increase the utility value of natural materials. In this study, adsorption performance was evaluated using kinetic studies to assess its potential for adsorbing Pb and MB. The evaluation was carried out using AAS and UV-Vis characterization. In addition, this study analyzed the structure, phase, functional groups, morphology, and surface area of nanocomposites using XRD, FTIR, SEM–EDX, and BET analysis.

Experimental Method

The synthesis of magnetite/activated carbon nanocomposites was carried out via the ex situ method. The first stage was the preparation of activated carbon, which began with grinding coconut shell charcoal and was followed by sieving through a 100-mesh sieve. Next, the coconut shell powder was calcined with N_2 at 400℃ for 5 hours. The calcined powder was reacted with 2 M KOH for 2 hours at 80℃ in a 1:5 ratio. The precipitate was then washed until the pH was neutral. The second stage was the synthesis of magnetite using the coprecipitation method, with steps following previously reported research [25]. The iron sand was cleaned, dried in the sun, and separated using a strong magnet to obtain Fe_3O_4 powder. Next, 20 grams of Fe_3O_4 powder was reacted with 37% HCl under stirring for 30 minutes at 720 rpm to form $FeCl_2$ and $FeCl_3$ solutions. The solution was then titrated with 25 mL of 25% NH4OH to form a magnetite precipitate. This reaction was carried out referring to Equations (1) and (2). The obtained magnetite precipitate was then washed to a neutral pH, followed by drying at 100 ^oC. The third stage was the synthesis of a magnetite/activated carbon nanocomposite, in which magnetite powder and activated carbon with a mass ratio of 40:3 were dissolved in 100 mL of deionized water under stirring for 1 hour at 720 rpm. The precipitate was then dried at 100 ^oC to obtain magnetite-activated carbon nanocomposite powder.

$$Fe_3O_{4(s)} + 8HCl_{(l)} \rightarrow 2FeCl_{3(l)} + FeCl_{2(l)} + 4H_2O_{(l)} \quad (1)$$

$$2FeCl_{3(l)} + FeCl_{2(l)} + 4H_2O_{(l)} + 8NH_4OH_{(l)} \rightarrow Fe_3O_{4(s)} + 8NH_4Cl_{(l)} + 8H_2O_{(l)} \quad (2)$$

The magnetite/activated nanocomposite was further characterized using XRD, SEM-EDX, FTIR, and BET to determine its structure, morphology, elemental content, functional groups, and total surface area and pore volume. Furthermore, a Pb adsorption test was carried out at pH 5 and an initial concentration of 23.23 ppm, while MB at pH 6 and an initial concentration of 14.73 ppm with an adsorbent dose of 0.05 g/25 mL, temperature of 27°C, stirrer speed of 650 rpm, and contact time variation of 5 to 30 minutes to determine the adsorption kinetics. Furthermore, adsorbent separation was performed using an external magnetic bar to attract the magnetite/activated carbon nanocomposite, after which the adsorbed Pb and MB solutions were characterized by AAS and UV–Vis spectroscopy. The adsorption standards reported in this study are adsorption efficiency and capacity, as well as adsorption kinetics to determine the adsorption rate and the time required to reach adsorption equilibrium.

Result and Discussion

The XRD results in Figure 1(a) show the diffraction pattern of the magnetite/activated carbon nanocomposite, refined using AMCSD 0007423 data. Magnetite diffraction peaks were

detected at 2θ = 30.3°, 35.5°, 43.8°, 57.4°, and 62.9° with hkl planes (220), (311), (400), (511), and (440). These diffraction peaks confirmed that the nanocomposite has an inverse cubic spinel structure with lattice parameters α = β = γ = 90°, which belongs to the Fd-3m space group, as illustrated in Figure 1(b). Magnetite nanoparticles consist of Fe^{3+} and Fe^{2+} ions, shown in blue, and O^{2-} ions, shown in yellow. Fe^{3+} ions occupy tetrahedral and octahedral positions, while Fe^{2+} ions occupy half of the octahedral positions [27]. Simultaneously, activated carbon particles expand at 2θ = 20–26° with low intensity and amorphous nature, so that magnetite nanoparticles dominate the diffraction of the nanocomposite [28]. Based on these results, the magnetite/activated carbon nanocomposite was successfully synthesized with high purity. Furthermore, the crystallite size and lattice parameters of magnetite were determined to be 11.03 nm and 8.353 Å, respectively.

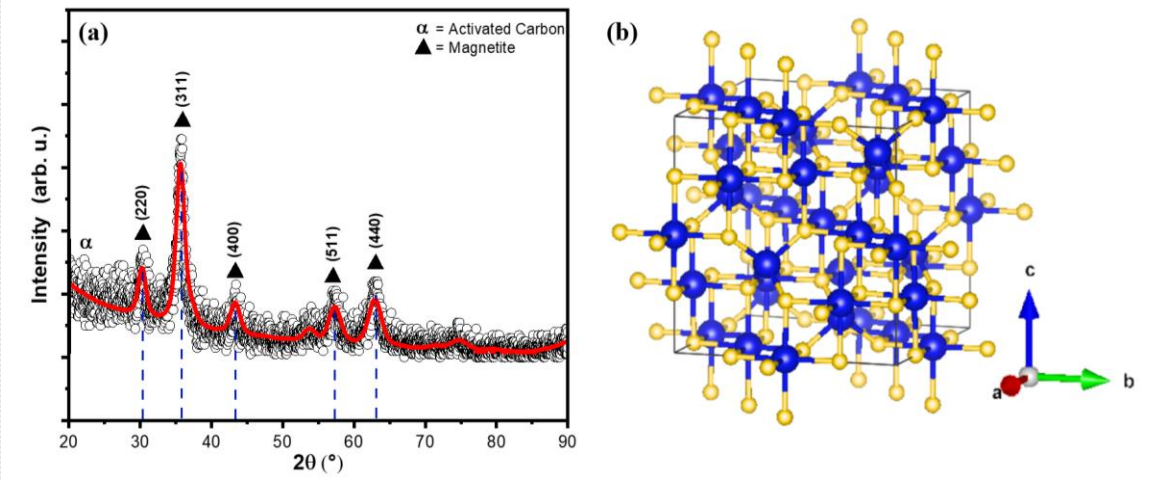

Figure 1. (a) Diffraction pattern of magnetite/activated carbon nanocomposites; and (b) crystal structure of magnetite

The morphology of the magnetite/activated carbon nanocomposite from SEM characterization with magnification of 100.000 times is shown in Figure 2(a). Magnetite nanoparticles are spherical and tend to agglomerate [29]. This is due to their relatively small size, which results in high surface energy and frequent particle collisions. As a result, the particles attract each other and condense to form secondary particles [30]. Meanwhile, the morphology of activated carbon is characterized by the presence of irregular pores as a matrix for magnetite growth [17]. Meanwhile, magnetite growth begins with Brownian motion, which is limited by the activated carbon surface due to its high surface energy. This condition is suitable for a magnetite dispersion medium [31,32]. As a result, the movement space of magnetite becomes limited, forming clusters, and magnetite impregnation occurs on the surface of activated carbon.

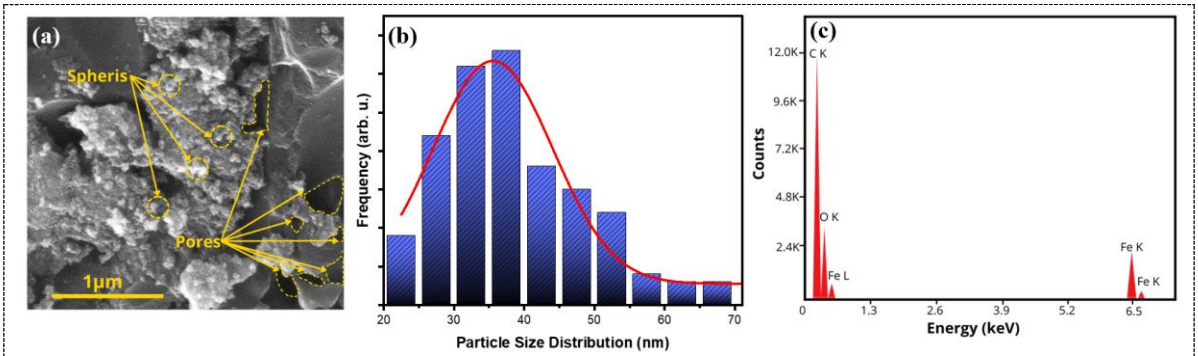

Figure 2. SEM images of (a) surface morphology at 100,000× magnification, (b) particle size distribution, and (c) EDX spectrum of magnetite/activated carbon nanocomposites

The average particle size distribution of the magnetic/activated carbon nanocomposite was determined to be 35.53 ± 0.83 nm, as shown in the histogram in Figure 2(b). The SEM particle size is larger than the XRD crystallite size because the XRD crystallite size indicates the size of a single crystal, while the SEM particle size indicates the size of particles (grains) composed of many single crystallites [33]. In addition, SEM characterization only shows the surface morphology of the nanocomposite, so that the observed size is not the primary particle but the aggregate size due to agglomeration [34,35]. Thus, the SEM particle size obtained is larger. Then, the EDX spectrum of the nanocomposite shown in Figure 2(c) detected iron (Fe) and oxygen (O) elements from magnetite, as well as carbon (C) element from activated carbon. This result is supported by previous studies, which reported that activated carbon consists of approximately 90% C elements, and magnetite consists of Fe and O [36]. This result is consistent with the XRD results, which show that the nanocomposite is composed solely of magnetite and activated carbon, with no impurities from other materials.

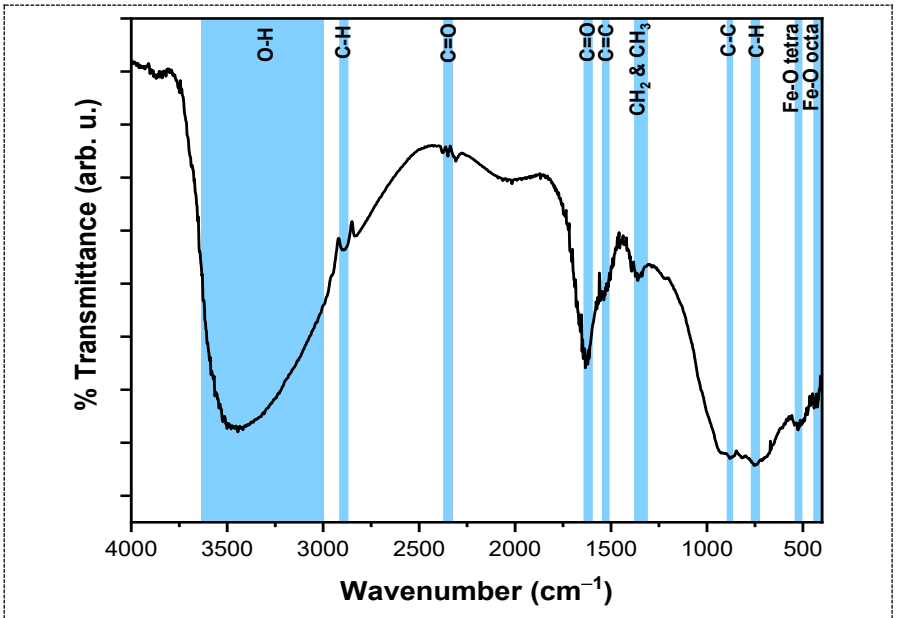

Figure 3. FTIR spectrum of magnetite/activated carbon nanocomposites

Figure 3 shows the FTIR spectrum of magnetite/activated carbon nanocomposite. The presence of magnetite nanoparticles was identified by Fe–O vibrations at 428 cm–1

(octahedral) and 523 cm–1 (tetrahedral) [37,38]. These two functional groups confirm that magnetite has an inverse cubic spinel structure $(Fe^{3+})_A[Fe^{2+}Fe^{3+}]_BO_4$ with trivalent ions in the tetrahedral and octahedral spaces, while all divalent ions occupy half of the octahedral space [39–42]. Furthermore, vibrations at 743 cm^{-1} and 2896 cm^{-1} were observed, which confirmed the cis C–H and C–H stretching bonds of activated carbon [43]. In addition, the vibrations of C–C, C–H (CH_2 and CH_3), C=C, and C=O at 873, 1351, 1533, 1621, and 2353 cm^{-1} also originate from activated carbon [44,45]. Furthermore, the presence of O–H groups at 3411 cm^{-1} indicates the stretching of hydroxyl groups on the surface of the nanocomposite [46].

Furthermore, the BET results showed that the magnetite/activated carbon nanocomposite had a specific surface area of 196.35 m^2/g with a total pore volume of 0.333 cm^3/g. Based on the IUPAC classification, the N_2 adsorption-desorption isotherm curve of the magnetite/activated carbon nanocomposite shown in Figure 4(a) corresponds to a type IV isotherm characterized by a hysteresis loop-shaped N_2 adsorption–desorption isotherm curve at a relative pressure (P/P_0) of 0.46–0.98. At low relative pressure, adsorption occurs in a monolayer on the nanocomposite surface. When the relative pressure is increased, adsorption occurs in a multilayer manner, and capillary condensation occurs. This IUPAC type IV curve also indicates that most of the nanocomposite pores are composed of mesopores (2–50 nm) [47]. This is reinforced by pore diameter distribution measurements using the BJH method, which show that the nanocomposite has an average pore diameter of 4.691 nm (Figure 4(b)).

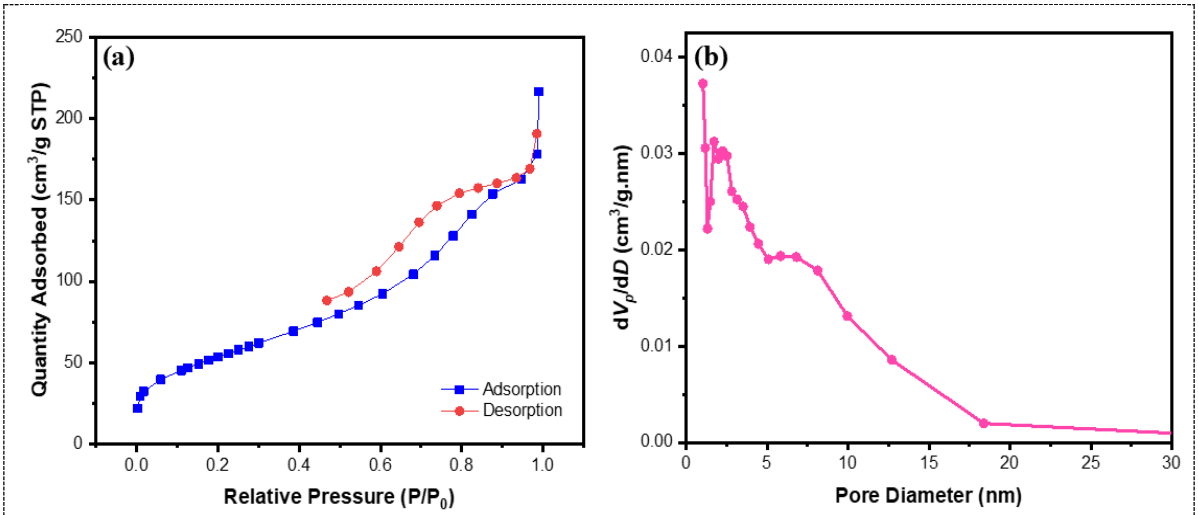

Figure 4. (a) N_2 adsorption–desorption isotherms; and (b) pore diameter of magnetite/activated carbon nanocomposites

Adsorption kinetics is the first step to evaluate in the adsorption process, as kinetic behavior determines the adsorption mechanism in magnetite/activated carbon nanocomposites. In this case, the adsorption performance can be studied using Equations (3) and (4) to find the adsorption efficiency and capacity.

$$R = \frac{C_i - C_f}{C_i} \times 100\% \quad (3)$$

$$q_e = \frac{(C_i - C_f) \times V}{W} \quad (4)$$

where R represents the adsorption efficiency (%), then C_i, C_f, and represent initial and final concentrations (mg/L), V represents volume (L), W represents mass of the reacted nanocomposite (g), and q_e represents adsorption capacity (mg/g).

Table 1. Initial concentration, final concentration, and adsorption efficiency of magnetite/activated carbon nanocomposites on Pb(II) and methylene blue.

Adsorbate	Contact time (minutes)	Initial concentration (ppm)	Final concentration (ppm)	Efficiency (%)
Pb(II)	5	23.23	1.040	95.54 ± 2.87
	10	23.23	0.330	98.56 ± 2.96
	15	23.23	0.310	98.68 ± 2.96
	20	23.23	0.220	99.05 ± 2.97
	25	23.23	0.110	99.51 ± 2.99
	30	23.23	0.100	99.56 ± 2.99
Methylene blue	5	14.73	0.629	95.73 ± 2.87
	10	14.73	0.851	94.22 ± 2.83
	15	14.73	0.748	94.93 ± 2.85
	20	14.73	0.438	97.02 ± 2.91
	25	14.73	0.559	96.19 ± 2.87
	30	14.73	0.776	94.74 ± 2.84

The results of the kinetic calculations of the lead and MB adsorption process are written in Table 1. The adsorption kinetics were investigated over a contact time of 5–30 minutes with an adsorbent dose of 0.05 g/25 mL and initial concentrations of lead and MB of 23.23 ppm and 14.73 ppm, respectively. Based on Table 1, the concentrations of Pb and MB in the solution decrease with increasing contact time, with the initial concentrations of 23.23 ppm for Pb and 14.73 ppm for MB decreasing to 0.100 ppm and 0.776 ppm, respectively, after 30 minutes of adsorption. This decrease confirms that Pb and MB in solution are adsorbed by the nanocomposite, thereby reducing contaminant concentration. Based on Figure 5(a), the adsorption performance of magnetite/activated carbon nanocomposites towards Pb(II) reached 95.54% in 5 minutes, then gradually increased to a balance point at 25 minutes, where it reached 99.51%. The increase in the adsorption value occurred because, at the contact time of 5 minutes, there were still active sites available for the nanocomposite to adsorb Pb(II) [48,49]. After 25 minutes, all active sites were fully occupied by Pb(II) ions, indicating saturation. Meanwhile, the adsorption of MB by the magnetite/activated carbon nanocomposite reached equilibrium at 20 minutes, with an adsorption performance of 97.02%, and decreased with increasing contact time (Figure 5(c)). This occurs because, at 20 minutes of contact time, all active sites are occupied by MB ions, so the nanocomposite surface is no longer able to bind the remaining MB ions. As a result, when the contact time is increased, some MB ions are released back from the nanocomposite surface, and the efficiency decreases [50].

In general, the adsorption kinetics were investigated using three models, namely pseudo-first order (PFO), pseudo-second order (PSO), and intra-particle diffusion following Equations (5), (6), and (7) [51].

$$log(q_e - q_t) = log\, q_e - K_1 t \quad (5)$$

$$\frac{t}{q_t} = \frac{1}{K_2 q_e^2} + \frac{1}{q_e} t \quad (6)$$

$$q_t = K_i t^{\frac{1}{2}} + c \quad (7)$$

where q_e and q_t represent adsorption capacity at the equilibrium point and specific time (mg/g), t for time (minutes), K_1, K_2, and K_i denotes the constants of the three kinetic models, and c represents the intersection point on the graph.

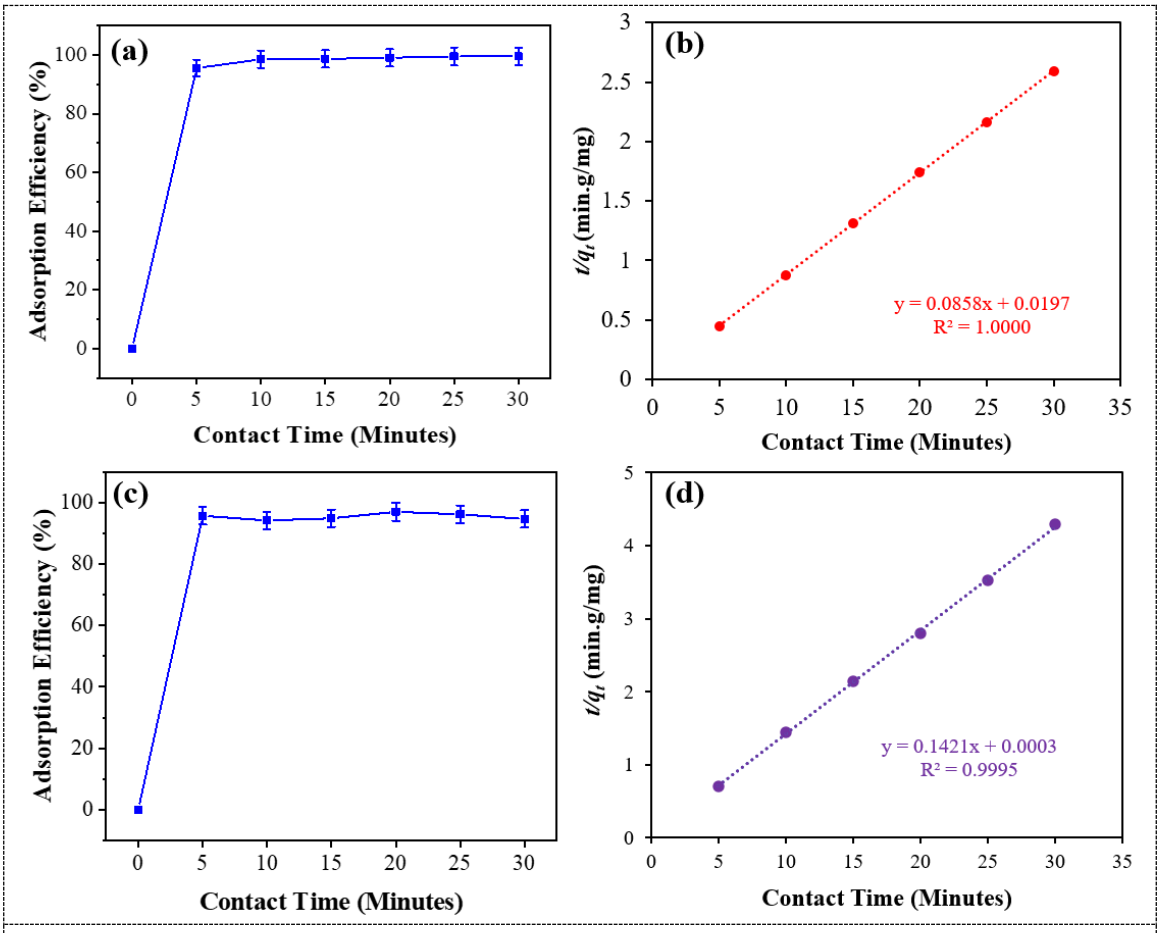

Figure 5. (a) Kinetics of Pb(II) adsorption with variations in contact time, (b) pseudo-second order (PSO) against Pb(II), (c) kinetics of methylene blue adsorption with variations in contact time, (d) pseudo-second order (PSO) against methylene blue with a dose of 0.05 g/0.025 L

Figure 5(b) and (d) show the PSO modeling results for Pb(II) and MB ions. Based on Table 2, the R^2 values for Pb(II) from PFO, PSO, and intra-particle diffusion modeling are 0.8629, 1.0000, and 0.7846, respectively, while for MB, the R^2 values are 0.0034, 0.9995, and 0.0276, respectively. The closer the R^2 value is to 1, or even equal to 1, the more accurate the kinetic model. Based on these results, the kinetics of magnetite/activated carbon nanocomposites fit the PSO model, in which the adsorption rate is proportional to the number of active sites on the nanocomposite surface [52]. PFO and PSO modeling here can only be used to investigate the rate-limiting step, and the involvement of physical or chemical interactions cannot be explained, as this requires further research on adsorption thermodynamics [53,54]. Furthermore, Table 2 shows that the adsorption capacities of Pb(II) and MB ions at

equilibrium are 11.6550 mg/g and 7.0373 mg/g, which are not much different from the experimental results of 11.5633 mg/g and 7.3513 mg/g. This shows the agreement between the experimental data and the theory. The results obtained in this study are higher than those from previous studies (Table 3).

Table 2. Comparison of parameter calculation results from adsorption kinetics modeling.

Adsorption	Kinetic model	Parameter	Value
Pb(II)	PFO	q_e (mg/g)	1.3198
		$q_{experiment}$ (mg/g)	11.5633
		k_1	0.0856
		R^2	0.8629
	PSO	q_e (mg/g)	11.6550
		$q_{experiment}$ (mg/g)	11.5633
		k_2	0.3737
		R^2	1.0000
	Intra-particle diffusion	$q_{experiment}$ (mg/g)	11.5633
		k	0.1284
		c	10.92
		R^2	0.7846
Methylene blue	PFO	q_e (mg/g)	0.1599
		$q_{experiment}$ (mg/g)	7.3513
		k_1	-0.0026
		R^2	0.0034
	PSO	q_e (mg/g)	7.0373
		$q_{experiment}$ (mg/g)	7.3513
		k_2	67.308
		R^2	0.9995
	Intra-particle diffusion	$q_{experiment}$ (mg/g)	7.3513
		k	0.0106
		c	6.9899
		R^2	0.0276

Several previous studies listed in Table 3 show magnetite adsorption capacities of 4.11, 1.07, and 0.67 mg/g [55,56]. Meanwhile, natural carbon-based adsorbent materials from clay honeycomb monolith, walnut shell, and chitin showed adsorption capacities of 1.14, 9.79, and 6.90 mg/g, respectively [57–59]. Magnetite/activated carbon nanocomposites adsorbed Pb at 11.66 mg/g and MB at 7.34 mg/g. These values are higher than the Pb adsorption capacity of commercial activated carbon of 10.77 mg/g [60]. In addition, the equilibrium time for Pb adsorption with the nanocomposite is faster, at 25 minutes, compared to 24 hours for commercial activated carbon (Table 3). This indicates that after adding magnetite, the adsorption capacity increases, classified as moderate. This increase in adsorption performance can be attributed to the irregular pore morphology of activated carbon (Figure 2). This pore irregularity leads to higher activation, thereby increasing the number of active sites [61]. With these active sites present, the adsorbate that diffuses into the pores of the activated carbon will bind to them and be adsorbed by the nanocomposite, thereby increasing the adsorption capacity. Furthermore, BET characterization results confirm that the nanocomposite has a high surface area, thereby increasing the surface or contact area available for adsorbing Pb and MB. Based on this, magnetite/activated carbon

nanocomposites are promising for wastewater treatment due to their high performance, abundant and inexpensive raw materials, and simple application. The application of magnetite/activated carbon nanocomposites does not require high temperatures; at 27 ℃, it can absorb >95% of Pb(II) and MB ions. Magnetite/activated carbon nanocomposites also exhibit magnetic properties that facilitate the separation of adsorbents from solutions, preventing them from becoming secondary pollutants.

Table 3. Comparison of magnetite/activated carbon nanocomposites with other adsorbents against Pb(II) and MB.

Adsorbent material	Adsorbate	Treatment	Adsorption capacity (mg/g)	Reference
Magnetite nanosphere	Pb(II)	pH 5, initial concentration 10 ppm, temperature 25℃, contact time 48 hours	4.11	[55]
Clay honeycomb monolith	Pb(II)	pH 4.5, initial concentration 30 ppm, dose 0.6 g/40 mL, temperature 25℃, contact time 150 minutes, stirrer speed 150 rpm	1.14	[57]
Walnut Shell	Pb(II)	pH 4, initial concentration 100 ppm, dose 1 g/250 mL, temperature 25℃, contact time 30 minutes, shaker speed 250 rpm	9.79	[58]
Commercial activated carbon	Pb(II)	Initial concentration 500 ppm, dose 2.5 g/50 mL, contact time 24 hours, stirrer speed 180 rpm	10.77	[60]
Magnetite nanoparticles modified with fig leaf extract	MB	pH 8, initial concentration 4 ppm, dose 0.05 g/20 mL, room temperature, contact time 30 minutes, stirrer speed 1500 rpm	1.07	[56]
Magnetite nanoparticles modified with azolla extract	MB	pH 8, initial concentration 4 ppm, dose 0.03 g/20 mL, room temperature, contact time 30 minutes, stirrer speed 1500 rpm	0.67	[56]
Chitin nanoparticles	MB	pH 6, initial concentration 10 ppm, dose 0.015 g/15 mL, temperature 25℃, contact time 30 minutes, stirrer speed 150 rpm	6.90	[59]
Magnetite/ activated carbon nanocomposite	Pb(II)	pH 5, initial concentration 23.23 ppm, dosage 0.05 g/25 mL, temperature 27℃, contact time 25 minutes, stirrer speed 650 rpm	11.66	This work
	MB	pH 6, initial concentration 14.73 ppm, dosage 0.05 g/25 mL, temperature 27℃, contact time 20 minutes, stirrer speed 650 rpm	7.34	

According to the PSO model, the adsorption rate is influenced by the active sites on the nanocomposite, such as the O–H and C=O groups detected in the FTIR spectrum. The O–H group is a negatively charged group that allows electrostatic interactions with the Pb(II) and MB cations. In addition to electrostatic interactions, there are other interactions in the adsorption of Pb(II), namely surface complexation and Pb^{2+}–π electron interactions [62–66]. This surface complexation will dominate Pb(II) adsorption, with the C=O and O–H groups binding to Pb(II) to form C=O–Pb and O–H–Pb. Meanwhile, the adsorption of MB occurs due to hydrogen bonds and π–π interactions [67–69]. Hydrogen bonds occur between the O–H group and the nitrogen atom of MB, and π–π interactions occur between the aromatic activated carbon structure and the benzene ring of MB. These interactions help mobilize Pb(II) and MB ions at the magnetite/activated carbon nanocomposite surface, enabling rapid adsorption onto its empty active sites. Once all adsorption sites have been filled, the Pb(II) and MB ions attached to the nanocomposite surface will gradually diffuse into the activated carbon pores until equilibrium is reached.

Conclusion

Magnetite/activated carbon nanocomposites have been successfully synthesized via coprecipitation. This success was confirmed by XRD, SEM-EDX, and FTIR results. XRD results show that magnetite has an inverse cubic spinel structure and activated carbon has an amorphous structure. The magnetite/activated carbon nanocomposite has a porous morphology, which is advantageous for adsorption because it provides numerous active adsorption sites. The pores were confirmed by BET with a total pore volume of 0.333 cm^3/g. In addition, the presence of O–H and C=O functional groups enhances the interaction of Pb(II) and MB ions with the nanocomposite surface, thereby increasing the adsorption potential. Furthermore, the adsorption analysis results showed that the magnetite/activated carbon nanocomposite reached equilibrium adsorption of Pb(II) ions at a contact time of 25 minutes, with an adsorption efficiency of 99.51% and a capacity of 11.6550 mg/g. Meanwhile, MB adsorption reached equilibrium at 20 minutes, with an adsorption efficiency of 97.02% and a capacity of 7.3421 mg/g. With these results, magnetite/activated nanocomposites derived from iron sand and coconut shells have great potential as adsorbents for lead and MB. To achieve optimal absorption performance, subsequent research should conduct a comprehensive study of adsorption parameters, including isotherms, thermodynamics, pH effects, and adsorbent dosage.

Acknowledgment

This research was funded by Kemdikbudristek of the Republic of Indonesia through the PPS-PTM scheme, contract number 2.6.155/UN32.14.1/LT/2025.

References

[1] P. Chandran *et al.*, "Biological treatment solutions using bioreactors for environmental contaminants from industrial wastewater," *J. Umm Al-Qura Univ. Appl. Sci.*, vol. 11, no. 2, pp. 185–207, 2025.
[2] BPS, "Statistik Lingkungan Hidup Indonesia: Air dan Lingkungan." Jakarta, 2020.
[3] A. M. H. Musthofa, M. Syafila, and Q. Helmy, "Effect of Activated Carbon Particle Size on Methylene Blue Adsorption Process in Textile Wastewater," *Indones. J. Chem.*, vol. 23, no. 2, p. 461, Apr. 2023.

[4] N. Nurjannah, N. Noralina, R. S. Oktari, and S.-J. Wang, "Elevated blood lead levels and associated risk factors among school children in a non-industrialized city in Indonesia," *PLOS One*, vol. 20, no. 10, p. e0332301, oct. 2025.
[5] N. Jagadeesh and B. Sundaram, "Adsorption of Pollutants from Wastewater by Biochar: A Review," *J. Hazard. Mater. Adv.*, vol. 9, p. 100226, Feb. 2023.
[6] B. Ericson, H. Hu, E. Nash, G. Ferraro, J. Sinitsky, and M. P. Taylor, "Articles Blood lead levels in low-income and middle-income countries : a systematic review," *Lancet Planet. Health*, vol. 5, no. 3, pp. e145–e153, 2005.
[7] S. Rajendran *et al.*, "A critical and recent developments on adsorption technique for removal of heavy metals from wastewater-A review," *Chemosphere*, vol. 303, no. March, pp. 1–14, 2022.
[8] M. Balali-mood, K. Naseri, Z. Tahergorabi, M. R. Khazdair, and M. Sadeghi, "Toxic Mechanisms of Five Heavy Metals: Mercury, Lead, Chromium, Cadmium, and Arsenic," *Front. Pharmacol.*, vol. 12, p. 643972, 2021.
[9] M. Islam, D. Roy, and D. Singha, "Metal Ion Toxicity in Human Body: Sources, Effects, Mechanisms and Detoxification Methods," *Chem. Afr. 2025 83*, vol. 8, no. 3, pp. 779–797, Mar. 2025.
[10] C. L. Bianchi, R. Djellabi, C. Della, and E. Falletta, "Doped-polyaniline based sorbents for the simultaneous removal of heavy metals and dyes from water: Unraveling the role of synthesis method and doping agent," *Chemosphere*, vol. 286, 2022.
[11] K. Rehman, F. Fatima, I. Waheed, and M. S. H. Akash, "Prevalence of Exposure of Heavy Metals and Their Impact on Health Consequences," *J. Cell. Biochem.*, vol. 119, no. 1, pp. 157–184, 2018.
[12] R. Foroutan, S. J. Peighambardoust, D. C. Boffito, and B. Ramavandi, "Sono-Photocatalytic Activity of Cloisite 30B/ZnO/Ag_2O Nanocomposite for the Simultaneous Degradation of Crystal Violet and Methylene Blue Dyes in Aqueous Media," *Nanomaterials*, vol. 12, no. 18, p. 3103, 2022.
[13] W. Siong *et al.*, "A review on conventional and novel materials towards heavy metal adsorption in wastewater treatment application," *J. Clean. Prod.*, vol. 296, p. 126589, 2021.
[14] R. Rashid, I. Shafiq, P. Akhter, M. J. Iqbal, and M. Hussain, "A state-of-the-art review on wastewater treatment techniques: the effectiveness of the adsorption method," *Environ. Sci. Pollut. Res.*, vol. 28, pp. 9050–9066, 2021.
[15] V. Russo, M. Hmoudah, F. Broccoli, M. R. Iesce, O. S. Jung, and M. Di Serio, "Applications of Metal Organic Frameworks in Wastewater Treatment: A Review on Adsorption and Photodegradation," *Front. Chem. Eng.*, vol. 2, no. October, pp. 1–13, 2020.
[16] J. O. Ighalo, F. O. Omoarukhe, V. E. Ojukwu, K. O. Iwuozor, and C. A. Igwegbe, "Cost of adsorbent preparation and usage in wastewater treatment: A review," *Clean. Chem. Eng.*, vol. 3, p. 100042, Sept. 2022.
[17] D. Das, D. P. Samal, and M. BC, "Preparation of Activated Carbon from Green Coconut Shell and its Characterization," *J. Chem. Eng. Process Technol.*, vol. 6, no. 5, p. 248, 2015.
[18] M. Ateia, D. E. Helbling, and W. R. Dichtel, "Best Practices for Evaluating New Materials as Adsorbents for Water Treatment," *ACS Mater. Lett.*, vol. 2, pp. 1532–1544, 2020.
[19] Y. Sukmono, R. A. Kristanti, B. V. Foo, and T. Hadibarata, "Adsorption of Fe and Pb from Aqueous Solution using Coconut Shell Activated Carbon," *Biointerface Res. Appl. Chem.*, vol. 14, no. 2, pp. 1–14, 2024.

[20] L. Soltys, O. Olkhovyy, T. Tatarchuk, and Mu. Naushad, "Green Synthesis of Metal and Metal Oxide Nanoparticles: Principles of Green Chemistry and Raw Materials," *Magnetochemistry*, vol. 7, no. 11, p. 145, Oct. 2021.
[21] R. Rahmawati *et al.*, "Green Synthesis of Magnetite Nanostructures from Naturally Available Iron Sands via Sonochemical Method," *Bull. Chem. Soc. Jpn.*, vol. 91, no. 2, pp. 311–317, Feb. 2018.
[22] Kh. Payandeh and S. Ghasemi, "Investigation of Kinetics and Equilibrium of Lead Absorbing Process by Magnetic Activated Carbon Powder with Fe_3O_4 Nanoparticles from Aqueous Solutions," *J. Water Wastewater*, vol. 30, no. 2, pp. 64–75, May 2019.
[23] D. Rao Vaddi, R. Malla, and S. Geddapu, "Magnetic activated carbon: A promising approach for the removal of methylene blue from wastewater," *Desalination Water Treat.*, vol. 317, p. 100146, Jan. 2024.
[24] J. Xu, Z. Liu, D. Zhao, N. Gao, and X. Fu, "Enhanced adsorption of perfluorooctanoic acid (PFOA) from water by granular activated carbon supported magnetite nanoparticles," *Sci. Total Environ.*, vol. 723, p. 137757, June 2020.
[25] D. Arista, A. Rachmawati, N. Ramadhani, R. E. Saputro, A. Taufiq, and Sunaryono, "Antibacterial Performance of Fe_3O_4/PEG-4000 Prepared by Co-precipitation Route," *IOP Conf. Ser. Mater. Sci. Eng.*, vol. 515, no. 1, 2019.
[26] A. Budianto, E. Kusdarini, W. Mangkurat, E. Nurdiana, and N. P. Asri, "Activated Carbon Producing from Young Coconut Coir and Shells to Meet Activated Carbon Needs in Water Purification Process Activated Carbon Producing from Young Coconut Coir and Shells to Meet Activated Carbon Needs in Water Purification Process," *J. Phys. Conf. Ser.*, vol. 2117, pp. 1–6, 2021.
[27] B. D. Cullity and C. D. Graham, *Introduction to Magnetic Materials*. Hoboken, USA: John Wiley & Sons, 2008.
[28] S. Wang, H. Nam, T. B. Gebreegziabher, and H. Nam, "Adsorption of acetic acid and hydrogen sulfide using NaOH impregnated activated carbon for indoor air purification," *Eng. Rep.*, vol. 2, no. 1, pp. 1–22, 2020.
[29] I. D. Fajariman *et al.*, "Comparative Behavior of Magnetic Iron Oxide Nanoparticles (MIONs) via Mechanical and Chemical Routes, Indonesian Physical Review, vol. 8, no. 1, p 181-195, 2025".
[30] M. D. Nguyen, H.-V. Tran, S. Xu, and T. R. Lee, "Fe_3O_4 Nanoparticles: Structures, Synthesis, Magnetic Properties, Surface Functionalization, and Emerging Applications," *Appl Sci*, vol. 11, p. 11301, 2021.
[31] C. M. Navarathna *et al.*, "Removal of Arsenic(III) from water using magnetite precipitated onto Douglas fir biochar," *J. Environ. Manage.*, vol. 250, p. 109429, Nov. 2019.
[32] J. P. Maity, P. R. Ho, Y. H. Huang, A. C. Sun, C. C. Chen, and C. Y. Chen, "The removal of arsenic from arsenic-bearing groundwater in In-situ and ex-situ environments using novel natural magnetic rock material and synthesized magnetic material as adsorbent: A comparative assessment," *Environ. Pollut.*, vol. 253, pp. 768–778, 2019.
[33] K. Shaik, V. K, and S. Cole, "Comparative Study of Crystallite Size from XRD and TEM Results for Pure and V_2O_5 Doped CdO-$FePO_4$ Composite Nanopowders," *Phys. Chem. Res.*, vol. 11, no. 2, June 2023.
[34] A. Taufiq *et al.*, "Fabrication of Fe3O4/SiO2/curcumin nanohybrid composites as new antifibrotic agents," *Chem. Pap.*, Mar. 2026.

[35] S. Modi, O. Okonkwo, H. Zhou, S. Kavadiya, M. Foston, and P. Biswas, "Geometric model for predicting the size and morphology evolution of multiparticle aggregates during simultaneous reaction and sintering," *Chem. Eng. J.*, vol. 458, p. 141423, Feb. 2023.
[36] A. Fadli, Komalasari, A. Adnan, Iwantono, Rahimah, and A. S. Addabsi, "Synthesis of Magnetite Nanoparticles via Co-precipitation Method," *IOP Conf. Ser. Mater. Sci. Eng.*, vol. 622, no. 1, p. 012013, Oct. 2019.
[37] N. P. Aulia, L. R. Herawati, ST. U. I. Subadra, A. Hidayat, Samian, and A. Taufiq, "Fabrication of Fe_3O_4/PVDF Magnetic Nanofiber Membranes for Magnetic Field Sensor," *J. Phys. Conf. Ser.*, vol. 2980, pp. 1–8, 2025.
[38] R. Jain and S. Gulati, "Influence of Fe^{2+} substitution on FTIR and Raman spectra of Mn ferrite nanoparticles," *Vib. Spectrosc.*, vol. 126, p. 103540, May 2023.
[39] V. Swathi Pon Sakthi Sri, Y. Aron Santhosh Kumar, M. Savurirajan, D. K. Jha, N. V. Vinithkumar, and G. Dharani, "Anticancer efficacy of magnetite nanoparticles synthesized using aqueous extract of brown seaweed Rosenvingea intricata, South Andaman, India," *Sci. Rep.*, vol. 14, no. 1, pp. 1–19, 2024.
[40] S. Khan *et al.*, "Antimicrobial activity of citric acid functionalized iron oxide nanoparticles –Superparamagnetic effect," *Ceram. Int.*, vol. 46, no. 8, pp. 10942–10951, June 2020.
[41] R. Rahmawati *et al.*, "Synthesis of Magnetite (Fe_3O_4) Nanoparticles from Iron Sands by Coprecipitation-Ultrasonic Irradiation Methods," *J. Mater. Environ. Sci.*, vol. 9, no. 1, pp. 155–160, 2018.
[42] Y. E. Gunanto, M. P. Izaak, E. Jobiliong, L. Cahyadi, and W. A. Adi, "High purity Fe_3O_4 from Local Iron Sand Extraction," *J. Phys. Conf. Ser.*, vol. 1011, no. 1, pp. 1–6, 2018.
[43] P. J. Wibawa, M. Nur, M. Asy'ari, and H. Nur, "SEM, XRD and FTIR analyses of both ultrasonic and heat-generated activated carbon black microstructures," *Heliyon*, vol. 6, no. 3, Mar. 2020.
[44] E. H. Sujiono *et al.*, "Fabrication and characterization of coconut shell activated carbon using variation chemical activation for wastewater treatment application," *Results Chem.*, vol. 4, no. November 2021, 2022.
[45] B. Kwasi Opoku, A. Isaac, A. Akrofi Micheal, J. Kwesi Bentum, and W. Paul Muyoma, "Characterization of Chemically Activated Carbons Produced from Coconut and Palm Kernel Shells Using SEM and FTIR Analyses," *Am. J. Appl. Chem.*, vol. 9, no. 3, p. 90, 2021.
[46] N. W. F. K. Wan, S. K. C. Soh, A. A. A. R. Azmi, M. S. M. Yusof, and M. Shamsuddin, "Synthesis and physicochemical properties of magnetite nanoparticles (Fe_3O_4) as potential solid support for homogeneous catalysts," *Malays. J. Anal. Sci.*, vol. 22, no. 5, pp. 768–774, 2018.
[47] S. Amornwutiroj, P. Manpetch, W. Singhapong, P. Srinophakun, and A. Jaroenworaluck, "Controllable synthesis of mesoporous magnetite/activated carbon composites as efficient adsorbents for hexavalent chromium removal," *J. Dispers. Sci. Technol.*, vol. 41, no. 10, pp. 1427–1444, 2020.
[48] E. I. Ugwu *et al.*, "Adsorption mechanisms for heavy metal removal using low-cost adsorbents: A review," *IOP Conf. Ser. Earth Environ. Sci.*, vol. 614, no. 1, 2020.
[49] P. M. Thabede, N. D. Shooto, and E. B. Naidoo, "Removal of methylene blue dye and lead ions from aqueous solution using activated carbon from black cumin seeds," *South Afr. J. Chem. Eng.*, vol. 33, pp. 39–50, July 2020.
[50] M. Kurnia, S. Suprapto, and Y. L. Ni'mah, "Bio-adsorbent for Remazol Brilliant Blue R (RBBR) dye," *South Afr. J. Chem. Eng.*, vol. 47, pp. 111–122, Jan. 2024.

[51] M. Alaqarbeh, "Adsorption Phenomena: Definition, Mechanisms, and Adsorption," *RHAZES Green Appl. Chem.*, vol. 13, no. September, pp. 43–51, 2021.
[52] G. William Kajjumba, S. Emik, A. Öngen, H. Kurtulus Özcan, and S. Aydın, "Modeling of Adsorption Kinetic Processes—Errors, Theory and Application," in *Advanced Sorption Process Applications*, S. Edebali, Ed., IntechOpen, 2019.
[53] J. Wang and X. Guo, "Adsorption kinetics and isotherm models of heavy metals by various adsorbents: An overview," *Crit. Rev. Environ. Sci. Technol.*, vol. 53, no. 21, pp. 1837–1865, Nov. 2023.
[54] D. Hermanto *et al.*, "FACILE SYNTHESIS OF ACTIVATED CARBON/ALGINATE/CHITOSAN COMPOSITE BEADS AS RHEMAZOLE BRILLIANT BLUE R ADSORBENT," *Indonesian Physical Review, vol. 7, no. 3, p 480-495, 2024*.
[55] M. Kumari, C. U. Pittman, and D. Mohan, "Heavy Metals [Chromium (VI) and Lead (II)] Removal from Water Using Mesoporous Magnetite (Fe3O4) Nanospheres," *J. COLLOID INTERFACE Sci.*, no. Vi, 2014.
[56] N. Alizadeh, S. Shariati, and N. Besharati, "Adsorption of Crystal Violet and Methylene Blue on Azolla and Fig Leaves Modified with Magnetite Iron Oxide Nanoparticles," *Int. J. Environ. Res.*, vol. 11, no. 2, pp. 197–206, 2017.
[57] M. Ahrouch, J. M. Gatica, K. Draoui, D. Bellido, and H. Vidal, "Lead removal from aqueous solution by means of integral natural clays honeycomb monoliths," *J. Hazard. Mater.*, vol. 365, pp. 519–530, Mar. 2019.
[58] H. Çelebi and O. Gök, "Evaluation of Lead Adsorption Kinetics and Isotherms from Aqueous Solution Using Natural Walnut Shell," *Int. J. Environ. Res.*, vol. 11, no. 1, pp. 83–90, 2017.
[59] S. Dhananasekaran, R. Palanivel, and S. Pappu, "Adsorption of Methylene Blue, Bromophenol Blue, and Coomassie Brilliant Blue by α-chitin nanoparticles," *J. Adv. Res.*, vol. 7, no. 1, pp. 113–124, 2016.
[60] R. Shahrokhi-Shahraki, C. Benally, M. G. El-Din, and J. Park, "High efficiency removal of heavy metals using tire-derived activated carbon vs commercial activated carbon: Insights into the adsorption mechanisms," *Chemosphere*, vol. 264, p. 128455, Feb. 2021.
[61] H. O. Orugba, J. E. Sinebe, J. L. Chukwuneke, V. I. Okoro, C. L. Enyi, and O. I. Ani, "Adsorption of cadmium from wastewater with activated carbons derived from pig fur biowaste: A comparative study of in-situ and ex-situ activation routes," *Heliyon*, vol. 10, no. 18, p. e37768, 2024.
[62] L. Qiu, C. Suo, N. Zhang, R. Yuan, H. Chen, and B. Zhou, "Adsorption of heavy metals by activated carbon: effect of natural organic matter and regeneration methods of the adsorbent," *Desalination Water Treat.*, vol. 252, pp. 148–166, Mar. 2022.
[63] C. Guo, J. Zou, J. Yang, K. Wang, and S. Song, "Surface characterization of maize-straw-derived biochar and their sorption mechanism for Pb^{2+} and methylene blue," *PLOS ONE*, vol. 15, no. 8, p. e0238105, Aug. 2020.
[64] J. Zhao, L. Wang, and G. Chu, "Comparison of the Sorption of Cu(II) and Pb(II) by Bleached and Activated Biochars: Insight into Complexation and Cation–π Interaction," *Agronomy*, vol. 13, no. 5, p. 1282, Apr. 2023.
[65] J. Wu, T. Wang, Y. Zhang, and W.-P. Pan, "The distribution of Pb(II)/Cd(II) adsorption mechanisms on biochars from aqueous solution: Considering the increased oxygen functional groups by HCl treatment," *Bioresour. Technol.*, vol. 291, p. 121859, Nov. 2019.

[66] S. Ambika *et al.*, "Modified biochar as a green adsorbent for removal of hexavalent chromium from various environmental matrices: Mechanisms, methods, and prospects," *Chem. Eng. J.*, vol. 439, p. 135716, July 2022.
[67] A. H. Jawad *et al.*, "Microporous activated carbon developed from KOH activated biomass waste: surface mechanistic study of methylene blue dye adsorption," *Water Sci. Technol.*, vol. 84, no. 8, pp. 1858–1872, Oct. 2021.
[68] N. S. Razali *et al.*, "High-Surface-Area-Activated Carbon Derived from Mango Peels and Seeds Wastes via Microwave-Induced $ZnCl_2$ Activation for Adsorption of Methylene Blue Dye Molecules: Statistical Optimization and Mechanism," *Molecules*, vol. 27, no. 20, p. 6947, Oct. 2022.
[69] J. Wang, Y. Tan, H. Yang, L. Zhan, G. Sun, and L. Luo, "On the adsorption characteristics and mechanism of methylene blue by ball mill modified biochar," *Sci. Rep.*, vol. 13, no. 1, p. 21174, Dec. 2023.